24th COBEM - 2017

24th ABCM International Congress of Mechanical Engineering
December 3-8, 2017, Curitiba, PR, Brazil

COBEM-2017-2875
AN EXPERIMENTAL STUDY ON THE STRUCTURAL BEHAVIOR OF A FLEXIBLE PIPE UNDER AXIAL COMPRESSIVE LOADS USING DIGITAL IMAGE CORRELATION

Rodrigo A. Amarante
Offshore Mechanics Laboratory, University of Sao Paulo
rodrigo.m.amarante@gmail.com

Celso P. Pesce
Offshore Mechanics Laboratory, University of Sao Paulo
ceppesce@usp.br

Rafael C. Santiago
Federal University of ABC
rafael.santiago@ufabc.edu.br

Roberto Ramos Jr
Offshore Mechanics Laboratory, University of Sao Paulo
rramosjr@usp.br

José Renato M. de Sousa
LACEO, Federal University of Rio de Janeiro
jrenato@laceo.coppe.ufrj.br

Marcos A. Rabelo
Federal University of Santa Catarina, Joinville
marcos.rabelo@ufsc.br

Abstract. *Due to compressive loads, flexible pipes may exhibit global and local structural instabilities and, consequently, structural failures. This work presents an experimental investigation concerning the local structural behavior of a 2.5-inch flexible pipe sample under compressive load. Instabilities of two types, elephant's foot buckling at the connector and radial (birdcaging) instability at mid sections, have been observed. Digital image correlation techniques, applied for the first time in this scenario, allowed a clear experimental assessment. Correspondence between axial compressive loads and observed instabilities are discussed. Further studies on triggering mechanisms for these two types of instabilities, aiming at proposing analytical stability criteria, are left to a further paper.*

Keywords: *flexible pipe, structural instability, radial buckling, birdcaging, elephant's foot buckling, compressive loads, experimental analysis, digital image correlation.*

1. INTRODUCTION

Compressive loads on flexible pipes and their consequent dynamic and structural effects have fundamental importance in offshore engineering. Such structures, used in offshore production of oil and gas, are composed by several concentric layers made of distinct materials – mainly metallic and polymeric ones - with different mechanical and geometric properties. Under compressive loads, flexible pipes may exhibit global and local structural instabilities and, consequently, structural failures. Among many kinds of structural instabilities flexible pipes may present, two are particularly important, associated with local

buckling, involving the helical wire tendons, strengthen helical tapes and the covering polymeric outer sheath. The first one happens at mid sections and can be of two types: wire birdcaging and wire lateral buckling. The second type may occur at the connectors and is known as elephant's foot buckling, as the outer polymeric sheath evolves to this kind of shape, after local bending yielding caused by end restriction effects. In fact, under axial compressive load, the helical wires tend to expand, causing internal radial loading on the surrounding layers. At mid sections, there are no restrictions to such an expansion other than the outer polymeric sheath and possibly a strengthen tape helically wounded around the wire armor layers. On the other hand, at the extremities of the pipe, radial constraints imposed by the metallic connectors induce local bending on the polymeric sheath.

The two phenomena of the first type have been extensively studied, and their deflagration mechanism is usually associated with the helical metallic wires layers, whose primary function is, in fact, to withstand tensile loads, not compressive ones. Usually, it is considered that under compressive loads, the wires may undergo local radial or 'lateral' buckling, characterized by a large radial expansion (grossly, in the principal normal direction) or lateral dislocations (grossly, in the bi-normal direction) of these helical structures, see, e.g., Sousa et al (2012), Malta and Martins (2014, 2015, 2016). Examples of such kind of structural instabilities are shown in Figure 1.

Figure 1: Examples of plastic deformations after instabilities caused by compressive loads in flexible risers. Upper left: 'wires lateral dislocations'; upper right: axisymmetric 'bubble' in the polymeric cover sheath; lower: 'wires birdcaging'. Source: Rabelo (2014), after Braga (2004).

However, another conjecture for the mechanism of radial instabilities deflagration has been raised in a recent study; Rabelo (2014) and Rabelo et al (2015). Per such a conjecture, radial instabilities at mid sections are triggered by the axisymmetric (radial) plastic instability of the external polymeric layer. Experimental tests and numerical models seem to corroborate such a conjecture. Rabelo et al (2015) developed analytical, numerical and experimental studies to investigate the axisymmetric instability of polymeric pipes under combined loads, axial compression and internal pressurization, used to withstand comparisons with numerical and experimental birdcaging investigations by Sousa et al (2012). The results obtained strongly indicate the conjecture validity.

The primary objective of the present work was, in fact, to ascertain Rabelo's (2014) birdcaging triggering mechanism conjecture; Rabelo et al (2015). For that, tests were planned and performed on 2.5-inch flexible pipe samples under pure compressive loads. Each sample was axially compressed and radial instabilities optically monitored, using a 3D digital image correlation (3D-DIC) technique, for the first time in the present scenario.

In fact, radial instabilities were observed in all experimental tests. However, due to the restrictions imposed by the connector to the sample end, another kind of radial instability, known as *elephant's foot buckling*, took place on the external polymeric sheath, preceding radial instabilities at mid sections. Despite the significance of such an experimental observation, a specific and detailed study related to the triggering mechanisms of both types of instabilities (elephant's foot buckling and birdcaging), as well as the proposition of a robust analytical criterion aiming at identifying the corresponding critical loads, will be left to a further article. Herein after, the main objective is to present the experimental results obtained using

3D digital image correlation techniques, by contrasting important aspects associated to the radial expansions observed in a flexible pipe sample with the axial compressive load history. This paper focus is therefore put on the new experimental assessment methodology.

2. THEORETICAL AND EXPERIMENTAL BACKGROUND

Structural mechanics of flexible pipes and umbilical cables have been under study for at least three decades. Analytical, numerical and experimental studies have been used in understanding birdcaging and related phenomena and their triggering mechanisms. Earlier, Sparks (1984), Witz and Tan (1992), Witz (1996), Taylor and Tran (1996) studied general aspects of such structures, both in theoretical and experimental ways. Further, works related to structural behavior of flexible pipes under combined loads were developed, e.g., Leroy and Estrier (2001), Novitsky and Sertã (2002), Braga (2004), Zhang et al (2003), Ramos (2001), Ramos and Pesce (2003, 2004), Bectarte and Coutarel (2004), Kaleff and Braga (2003) and Custódio (2005), to mention a few. Braga (2003) performed a detailed experimental study about the instability of the helical armors of a flexible pipe and evaluated its behavior under cyclic loading. Zhang et al (2003) presented analytical tools for the optimization of unbounded flexible tubes under different load conditions. Vaz and Rizzo (2011), Sousa et al (2012), Sertã et al (2012), Saevik and Thorsen (2012) and Saevik and Guomin (2014), worked on birdcaging issues using numerical codes. Sousa et al (2012) compared experimental data with computational simulations with high representativeness and acuity. Malta and Martins (2014) noted axial compressive loads in tension armors and investigated radial instabilities due to pressure variations. A numerical 3D model (finite element method based) was developed and several case-studies were presented. Effects of model length and friction between layers were assessed as well; see Malta and Martins (2015, 2016). Following another way of reasoning, Rabelo (2014) developed a birdcaging deflagration criterion, conjecturing that the axisymmetric structural instability of the outer polymeric layer plays a fundamental role in the birdcaging triggering; see also Rabelo et al (2015).

From another side, related to elephant's foot buckling, the works by Legget (1946), Batterman (1965), Rotter (2006), Bardi and Kyriakides (2006a,b) and Dhar and Muntakim (2015) are particularly important.

3. EXPERIMENTAL PROCEDURES

Experimental tests were performed at the Offshore Mechanics Laboratory (LMO-USP), using a MTS250kN universal test rig. A steel frame (Figure 2) was specially designed and built to hold a 2.5-inch flexible pipe sample by its ends. At the sample's top end, a squared-shape steel plate is attached, screwed in a steel cylindrical bar (passing through riser's internal tube, in light blue, Figure 2).

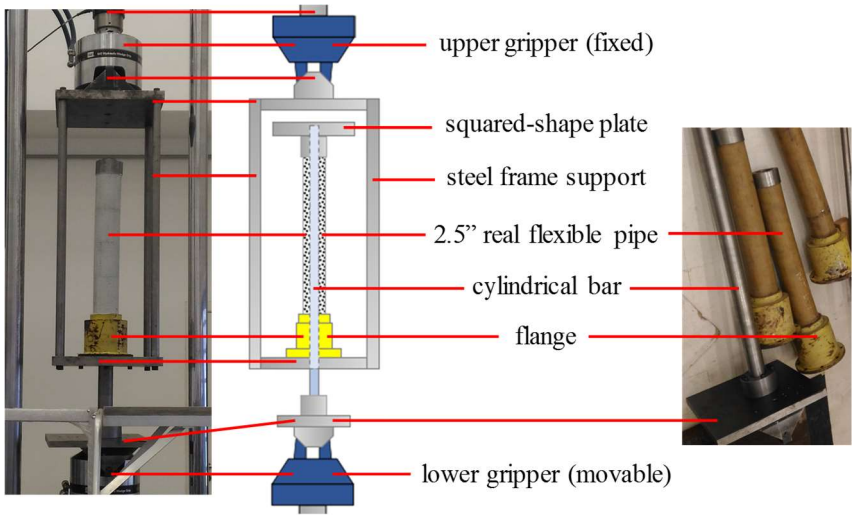

Figure 2: Steel frame designed to support the flexible pipe in the compression tests.

During the tests, the upper gripper (in dark blue color at the top of Figure 2, at center) remained in a fixed position, while the lower gripper (in dark blue color at the bottom of Figure 2, at center) moved downwards vertically. The compressive load is then applied to the upper end of the sample (attached in a flange, Figure 2 at right), by pulling an internally guiding cylindrical bar (in light blue color at Figure 2, at center), gripped to the hydraulic lower head, that passes through the pipe. The lower gripping mechanism is free to twist around the vertical axis.

The experiments were designed for 3D optical monitoring, which is simpler and able to cover an entire surface, with much larger area than commonly used techniques based on regular strain gauges. This optical monitoring system can measure the displacements and strain fields on the flexible pipe external plastic sheath, from a special surface painting: a white background with black pigmentations, as illustrated in Figure 4 (at center and highlighted at left). The basic procedure of the image capture consists in determining the position of each agglomerated black pixel of an image, relative to its initial position, with respect to its actual location in the next frame, using digital image correlation algorithms; see Schreier et al (2009).

Two synchronized cameras were used to 3D monitoring (Fig.3, at bottom), preceded by calibration procedures, performed before each test (as illustrated at Fig. 4, at right). This procedure transforms image into coordinates systems. Accuracy is about hundredths of one millimeter.

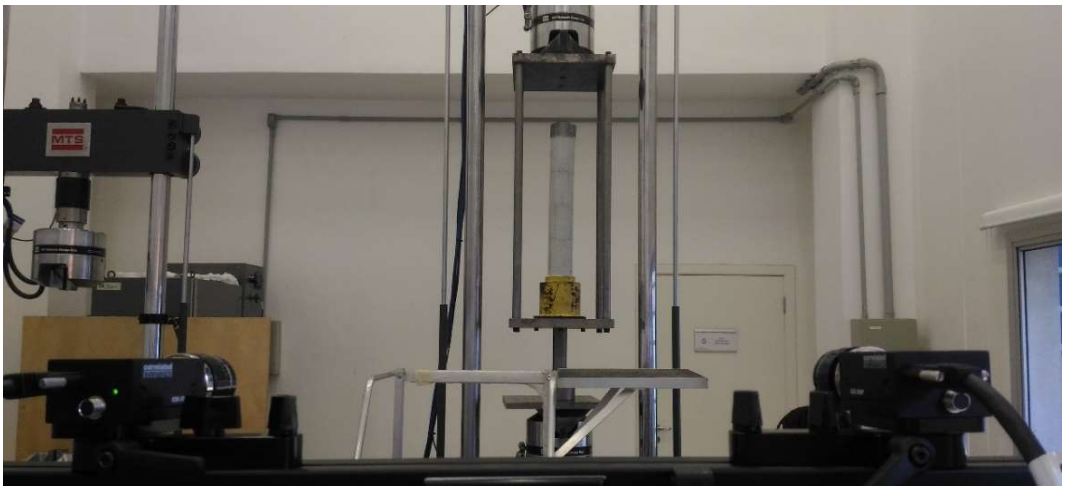

Figure 3: Experimental apparatus from optical monitoring system's point of view.

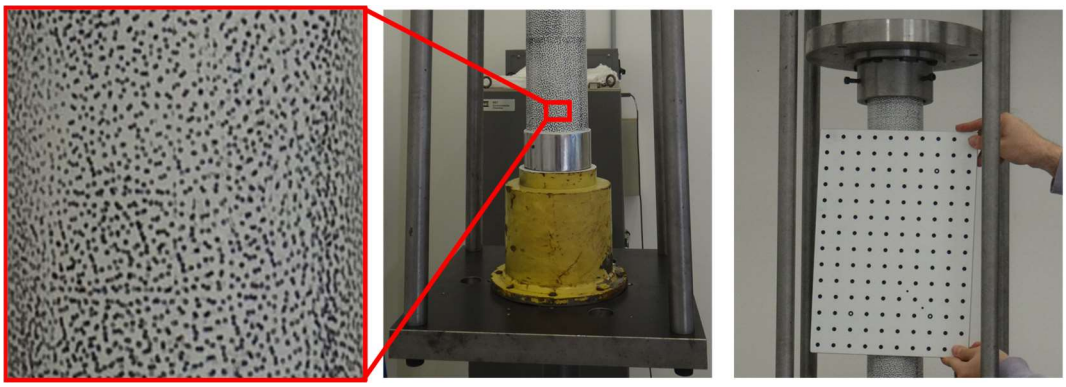

Figure 4: Details of the painted flexible pipe mounted in the steel frame, ready for calibration and testing.

For test planning and further analysis, the cover sheath material, polyamide-12, was mechanically characterized in the Center for Materials Characterization and Development (CCDM, Federal University of Sao Carlos), for further experimental analysis. For the mechanical characterization tests, samples were made from a 1000mm long polymeric sheath piece, drawn from one of the flexible pipes available, as illustrated in Figure 5. Another 250mm long piece was taken and samples prepared to evaluate orthogonal properties. The tests included the determination of viscoelastic properties, including relaxation and creep.

Figure 5: Sample of the outer polymeric sheath used to characterization tests.

For the compressive tests, 500mm long samples were made from the flexible pipe. This pipe is a five layers structure (see Figure *6*), whose properties (mean values) are listed in Table 1. From the innermost to the outermost layer, the numbering in Fig. 6 refers to: (1) interlocked steel carcass; (2) pressure plastic sheath (liner); (3) internal tensile armor layer; (4) external tensile armor layer; and (5) external plastic sheath (polyamide-12); Ramos et al, (2015). Note that this particular flexible pipe is not a riser, but a flow-line designed for relatively small depths. In this design a reinforcing strengthen tape, usually wounded around the helical armor layers for birdcaging prevention, is absent. Therefore, the external helical armor layer exerts a direct internal radial loading on the external polymeric sheath, caused by the radial expansion of both armor layers when the pipe is subjected to compressive loads.

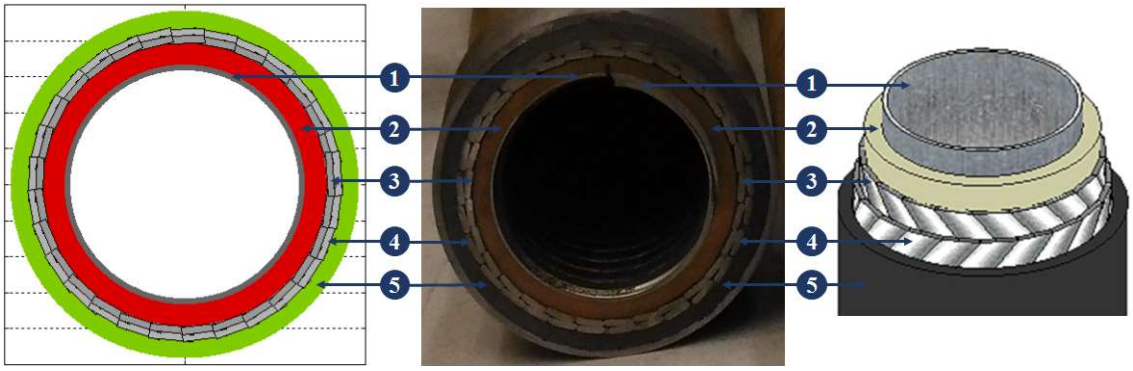

Figure 6: Identification of the flexible pipe layers; at left, 2D structural section (PipeDesign©[1]); at center, real pipe; at right, 3D structural layers (PipeDesign©).

Table 1: As-built original properties of the materials of each flexible pipe layer

Layer	Properties						
	E	ν	D_i [mm]	D_o [mm]	n	α (deg)	t [mm]
1	190 GPa	0.3	63.50	66.76	1	85.8	1.63
2	280 MPa	0.45	66.76	78.76	1	-	6.00
3	207 GPa	0.3	78.76	82.76	29	55.5	2.00
4	207 GPa	0.3	82.76	86.76	29	-55.5	2.00
5	320 MPa	0.45	86.76	96.76	1	-	5.00

In Tab. 1 "E" refers to Young's modulus, "ν" is the Poisson's ratio, "D_i" and "D_o" represent inner and outer diameter, respectively, "n" is the number of elements per layer, "α" is the angle of the wire with respect to the axis of the flexible pipe and "t" is the thickness of the corresponding layer.

During the experimental planning, to evaluate the axial compressive birdcaging buckling load, computational simulations were carried out using an in-house program based on analytical models by Ramos and Pesce (2004). The modelling considered the complete geometry of the flexible pipe, including all internal layers (Figure 6 at left), as well as its geometric and mechanical properties.

4. RESULTS AND DISCUSSION

By controlling displacements imposed by the test rig, the flexible pipe sample was axially compressed. Three samples were assayed. The results presented in this paper refer to only one of the samples. In order to assess boundary conditions at the ends of the pipe, the displacements of points in the vicinity of the terminations were measured.

The graphic shown in Fig. 7 refers to a point at the upper end of the sample. As expected, the most significant displacements appear in the vertical (axial) direction V (see reference frame at Fig. 7 at left), consistently to the imposed compressing loading. Very small displacements in the U and W directions occurred in this region due to the tight support connected at that end, as can be seen in the corresponding graphs. Downward displacements applied to the sample top end resulted in axial compressive loads, as illustrated in in Fig. 8. Differently from typical curves of similar tests with common pipes, several points deserve attention and discussion, which will be presented below.

[1] For further information about PipeDesign© analytical models, see Pesce and Ramos Jr, 2009.

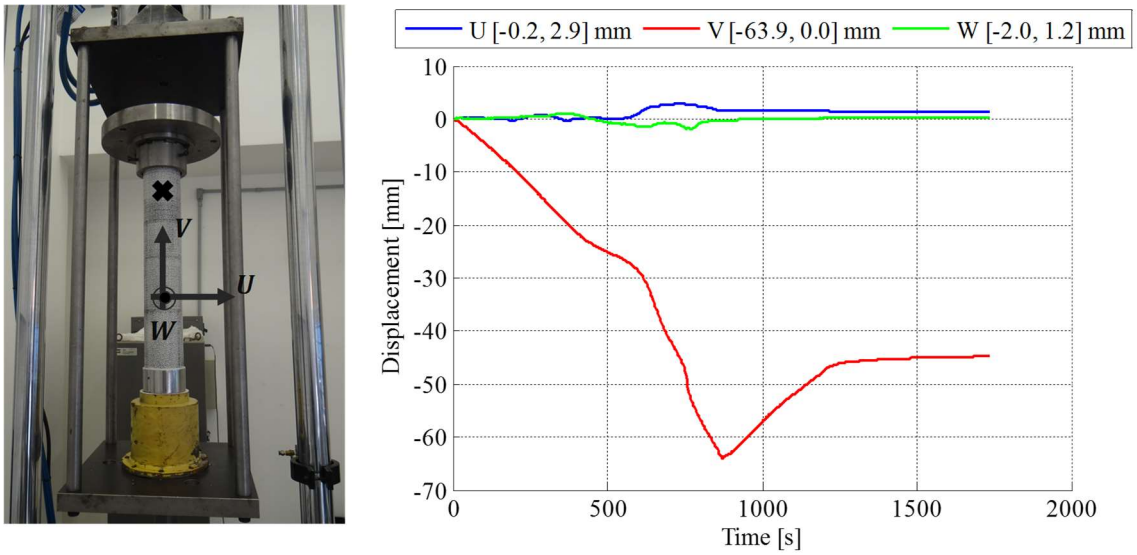

Figure 7: Measured displacements, with respect to the global fixed reference axes (on the cameras), of a point located nearby the upper end of the riser (marked with a black color cross at left).

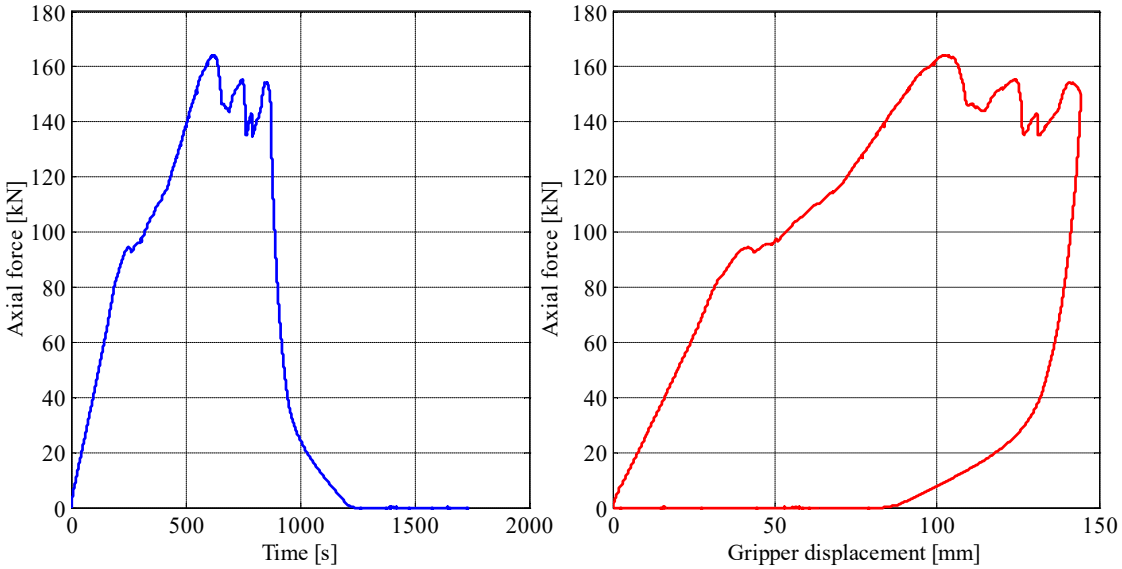

Figure 8: Compressive force applied at the ends of the sample as function of time (left) and of gripper displacement.

Notably, there is an evident reduction in the compressive axial stiffness of the pipe sample between instants 200s and 300s, as well as peculiar oscillations in the curve between the instants 600s and 900s. Additionally, in the unloading phase, a typical viscoelastic behavior, due to the external polymeric sheath is evident. As a matter of fact, for this particular flexible pipe, the external polymeric sheath attains circa 52.3% of the whole compressive load, as shown in Tab. 2. In this table, F is the total axial compressive load and F_i is the parcel supported by the i-th layer (see Fig. 6); $pc_{,ij}$ is the interfacial pressure between layers i and j.

Interfacial pressure values were numerically determined, using Ramos and Pesce (2004) analytical modeling procedures. However, much more important than having visual perceptions is the need of understanding the causes of such peculiarities and their association with the large radial deformations observed over the riser sample.

Anticipating further explanations, the ultimate plastic deformations observed in Fig. 9 at left are color-coded with the time intervals of the diagram at right and hence to the corresponding compressive loads.

Table 2: Compressive load distribution and interlayers pressure. Results from numerical simulation

F (kN)	F_1 (kN)	F_2 (kN)	F_3 (kN)	F_4 (kN)	F_5 (kN)	$pc,_{12}$ *(kPa)*	$pc,_{23}$ *(kPa)*	$pc,_{34}$ *(kPa)*	$pc,_{45}$ *(kPa)*
0	0	0	0	0	0	0	0	0	0
-10	-0.001	-4.5	-0.1	-0.2	-5.2	0	0	7.0	21.1
-20	-0.002	-9.0	-0.3	-0.3	-10.4	0	0	14.0	42.2
-30	-0.003	-13.4	-0.4	-0.5	-15.7	0	0	21.0	63.3
-40	-0.004	-17.9	-0.5	-0.6	-20.9	0	0	27.9	84.4
-50	-0.004	-22.4	-0.7	-0.8	-26.1	0	0	34.8	105.6
% F	0.0%	44.8%	1,3%	1.6%	52.3%				

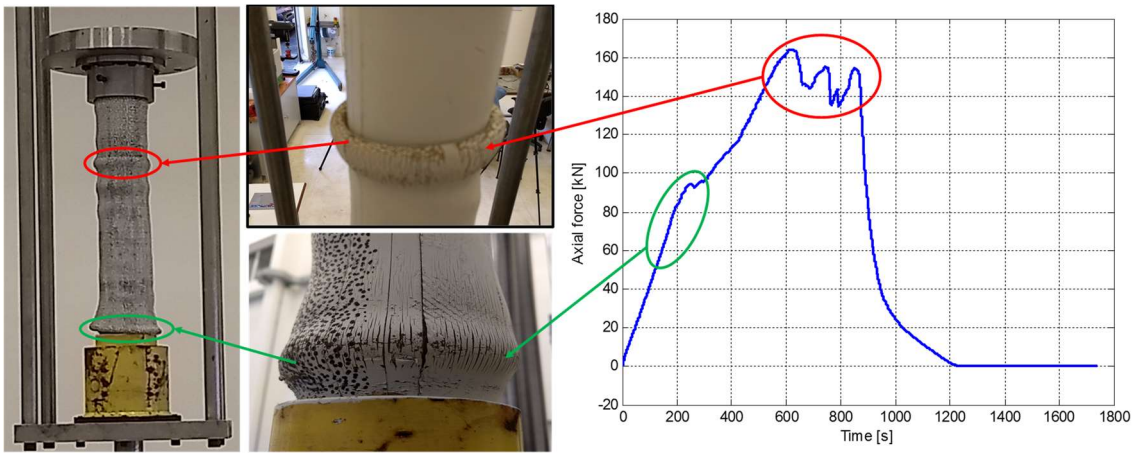

Figure 9: Radial instabilities of outer polymeric sheath and associated axial loads.

For a preliminary understanding of these statements, refer to Fig. 10, where 10 groups of three pictures (designated “a” to “j”) is presented, at selected instants. The left picture of each group corresponds to the time series of the axial compressive load applied on the riser. The marker ("o") is associated with the axial load at the instant under consideration. Horizontal and vertical errors bars, plotted in red color, correspond to errors due to a very small time-lag observed between the 3D-DIC system and the MTS250kN controller.

The central figure of each group shows a picture taken by the monitoring system at that instant, in which radial deformations fields on the polymeric outer sheath may be visualized. The color bar scale at the bottom of the figure gives the radial displacement field measure, in millimeters, relative to the values before loading. The third figure of each frame, the right one, represents a longitudinal profile of the radial displacement measured at the outer diameter of the polymeric sheath, in the horizontal (W) direction. The radius profile is identified by the same color of the respective marker at the left graph. Radial displacements are measured with respect to the non-deformed profile. Horizontal lines represent the limits of the lower and upper sections of the pipe. The lower one is fixed and represented in light gray color; the upper one is given in green, at the initial position and red, in the final position, at maximum compression. Vertical light gray line represents the initial profile.

Frames sequence in Fig. 10 begins just before loading. The two subsequent frames represent the beginning of the axial loading and the first perceptions of radial deformations, which are more noticeable in frame “d”, where there is a clear radial expansion, possibly still elastic. Circular marker in Figure "e" corresponds to the instant of a clear transition in the compressive stiffness values. The radial displacement profile observed along the length of the sample induces a possible birdcaging triggered by the first radial buckling. Elephant’s foot buckling is evident and the radial deformation in this region is surely plastic.

In the sequence, it is possible to observe, in the frames "f" and "g", an abrupt radial expansion followed by plastic deformation, until the maximum compressive load on the riser is reached. So far, the axial structural behavior is predominantly elastoplastic. After this maximum load point, axial load values oscillate while imposed displacements remain increasing at the same rate. These oscillations are evidently associated with the plastic sheath wrinkling, clearly noticeable in the region where birdcaging started. The radial expansion reaches its maximum, the polyamide thickness reduces and the large axisymmetric bump folds onto itself. Frames “g” to “i” correspond to the events last described. The last frame corresponds to the maximum displacement, just before the unloading phase.

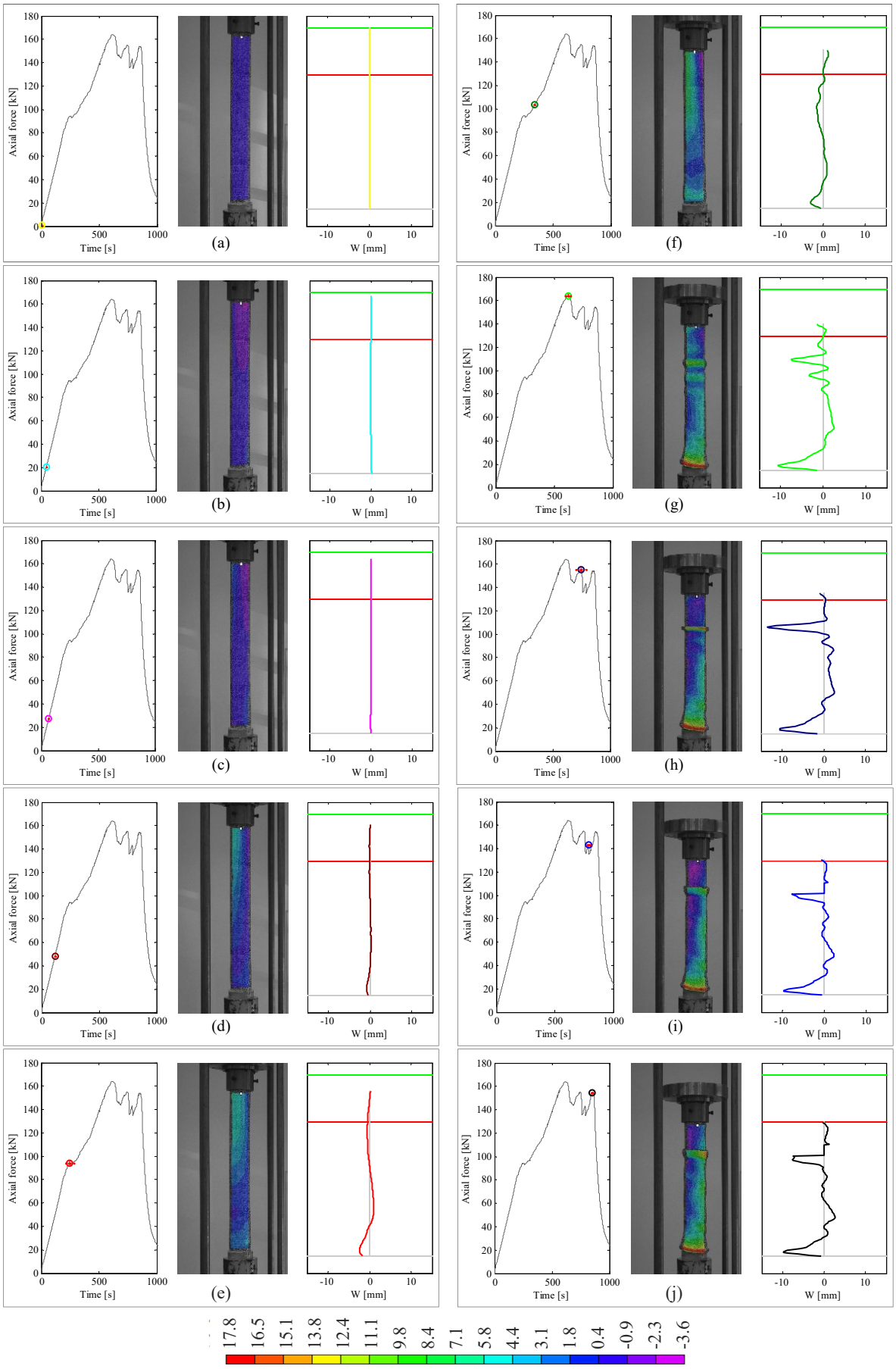

Figure 10: Time evolution (a to j) of the compressive axial load (left), 3D-DIC displacement field measurement, (picture at center) and the radial displacement profile of the polymeric external sheath of the flexible pipe (right). The colormap indicates the radius variation, in millimeters.

5. CONCLUSIONS

Occurrence of axial compressions in flexible pipes, although undesirable, is evidenced throughout its service life. As a consequence, global and local instabilities can be verified, compromising the performance and integrity of these structures. Radial instabilities may occur, leading to considerable radial expansions. Numerous studies have been carried out under the hypothesis that such instabilities are triggered by outer and inner tensile armor layers. However, the conjecture that the outer polymeric sheath is, in fact, the first trigger for the occurrence of birdcaging has been evidenced experimentally and grounded this work.

Using 3D optical monitoring, especially associated with digital image correlation techniques, was fundamental for obtaining the presented results, allowing to highlight aspects previously uninvestigated. Accurate visualization of axial and radial deformations in real time, and its association to the axial loads and respective structural instability were only possible due to this advanced optical tracking measuring technique.

The experimental results obtained so far, like elephant's foot deflagration, concomitantly to birdcaging, demand additional researches, based on analytical formulations, numerical methods and on the construction of theoretical instability diagrams. This has been left for a further paper. Complementary, another experimental campaign has been planned, to test flexible pipe samples provided with compliant end terminations, aimed at avoiding elephant`s foot buckling to occur before the onset of birdcaging.

6. ACKNOWLEDGEMENTS

We are especially grateful to Dr. José Donato Ambrósio and MSc Rubens Eduardo dos Santos, CCDM/Ufscar. Authors also thank the National Council for Scientific and Technological Development (CNPq) for a postdoctoral scholarship - processes # 402975/2014-6 and 158069/2015-3 - and the research grants - PQ 308990/2014-5 and PQ 308403/2016-9 - essential for the accomplishment of this work and those that will follow.

7. REFERENCES

Bardi, F.C., Kyriakides, S. “Plastic buckling of circular tubes under axial compression, part I: Experiments”, International Journal of Mechanical Sciences, Vol. 48, Issue 8, pp 830-841, 2006.

Bardi, F.C., Kyriakides, S. “Plastic buckling of circular tubes under axial compression, part II: Analysis”, International Journal of Mechanical Sciences, Vol. 48, Issue 8, pp 842-854, 2006.

Batterman S.C. "Plastic buckling of axially compressed cylindrical shells", AIAA Journal, Vol. 3, No. 2, pp. 316-325, 1965.

Bectarte, F., Coutarel, A., “Instability of tensile armour layers of flexible pipes under external pressure”, Proceedings of OMAE2004 conference, Vancouver, 2004.

Braga, M.J.P., “Instabilidade de Armaduras de Tração de Linhas Flexíveis”. Relatório Final RT TMEC No 011/2004 (restricted, in Portuguese). CENPES/PDP/TMEC, Rio de Janeiro, 65p, 2004.

Custódio, A.B., “Modelo analítico para estimativa de falha por instabilidade em armaduras de dutos flexíveis”. Doctoral thesis (in Portuguese). COPPE/UFRJ, 2005.

Dhar, A.S., Muntakim, A.H. “Nonlinear analysis of axisymmetrically wrinkled pipes under axial loads and internal pressures”, 34th International Conference on Ocean, Offshore and Arctic Engineering, 2015.

Kaleff, P., Braga, M.P., “Flexible pipe sensitivity to birdcaging and armour wire lateral buckling”, Proceedings of OMAE2004, 23rd International Conference on Offshore Mechanics and Arctic Engineering, 2004.

Legget, D.M.A. “The buckling of thin shells under axial compression”, 6th International Congress of Aplied Mechanics, 1946.

Leroy, J.M., Estrier, P., “Calculations of stresses and slips in helical layers of dynamically bend flexible pipes”, Oil and Gas Science and Technology, vol. 56, n. 6, 545-554, 2001.

Malta, E.R., Martins, C.A., “Finite element analysis of flexible pipes under compression”, Proceedings of the 33rd Conference on Ocean, Offshore and Arctic Engineering, OMAE2014-23192, 2014.

Malta, E.R., Martins, C.A., “Finite element analysis of flexible pipes under compression: influence of the sample length”, Proceedings of the 34th Conference on Ocean, Offshore and Arctic Engineering, OMAE2015-42043, 2015.

Malta, E.R., Martins, C.A., “Finite element analysis of flexible pipes under compression: influence of the friction coefficient”, Proceedings of the 35th Conference on Ocean, Offshore and Arctic Engineering, OMAE2016-54895, 2016.

Novitsky, A., Sertã, S., “Flexible pipes in Brazilian ultra-deepwater fields – a proven solution.”, Proceedings of the 14th deep offshore technology, Riser Technology Symposium, New Orleans, 2002.

Pesce, C.P., Ramos Jr, R. “Modelos Analíticos em Mecânica-Estrutural de Tubos Flexíveis: Distribuição de Esforços Solicitantes em Seções de Tubos Flexíveis: Modelos de Segunda Geração sob Tração, Torção e Flexão” (in Portuguese). Technical Report RT-SM06-Rev 01, LMO-USP, Prysmian Project on Flexible Pipes Design Methodology Development, Phase 1, january, 2009, 59p.

Rabelo, M.A. “Investigação sobre a instabilidade axissimétrica de tubos de polietileno de alta densidade sujeitos a compressão axial e pressurização interna e um critério de previsão do fenômeno de ‘birdcaging’ em tubos flexíveis”. Doctoral thesis (in Portuguese). University of Sao Paulo, Sao Paulo, Brazil, 2014.

Rabelo, M.A., Pesce, C.P.; Santos, C.C.P., Ramos JR, R.; Franzini, G.R., Gay Neto, A. “An Investigation on Flexible Pipes Birdcaging Triggering”. Marine Structures, vol. 40, 159-182, 2015.

Ramos Jr, R., “Modelos Analíticos no Estudo do Comportamento Estrutural de Tubos Flexíveis e Cabos Umbilicais”. 2001. Doctoral thesis (in Portuguese). University of Sao Paulo, Sao Paulo, Brazil, 2001.

Ramos Jr, R., Pesce, C.P., “A stability analysis of risers subjected to dynamic compression coupled with twisting”, Journal of Offshore Mechanics and Arctic Engineering, vol. 125, 183 - 189, 2003.

Ramos Jr, R., Pesce, C.P., “A consistent analytical model to predict the structural behavior of flexible risers subjected to combined loads”, Journal of Offshore Mechanics and Arctic Engineering, vol. 126, pp. 141 -146, 2004.

Ramos Jr, R., Martins, C.A., Pesce, C.P., Roveri, F.E. “Some Further Studies on the Axial–Torsional Behavior of Flexible Risers”. Journal of Offshore Mechanics and Arctic Engineering, vol. 136, 011701-1, 2014.

Rotter, J.M. “Elephant’s foot buckling in pressurised cylindrical shells”, Stahlbau, Vol. 75, Heft 9, pp. 742-747, 2006.

Schreier, H., Orteu, J. J., & Sutton, M. A. “Image correlation for shape, motion and deformation measurements”. Springer US, 2009.

Sousa, J.R.M., Viero, P.F., Magluta, C., Roitman, N. “An experimental and numerical study on the axial compression response of flexible pipes”. Journal of Offshore Mechanics and Artic Engineering (JOMAE), 2012.

Sparks, C.P., “The influence of tension, pressure and weight on pipe and riser deformations and stresses”, Transactions of the ASME, vol. 10, p. 46 – 54, 1984.

Taylor, N., Tran, V., “Experimental and theoretical studies in subsea pipeline buckling”, Marine Structures, vol. 9, p. 211 – 257, 1996.

Vaz, M.A.; Rizzo, N.A.S. “A finite element model for flexible pipe armor wire stability”, Marine Structures, vol. 24, issue 3, p. 275 – 291, 2011.

Witz, J.A. “A case study in the cross-section analysis of flexible pipes” – Marine Structures – vol. 9 – pp. 885 – 904, 1996.

Witz, J.A., Tan, Z., “On the axial-torsional structural behaviour of flexible pipes, umbilicals and marine cables”, Marine Structures, Barking, vol. 5, p. 205-227, 1992.

Zhang, Y., Chen, B., Qiu, L., Hill, T., Case, M., “State of the art analytical tools improve optimization of unbounded flexible pipes for deepwater environments”, Offshore Technology Conference, 2003.

8. RESPONSIBILITY NOTICE

The authors are the only responsible for the printed material included in this paper.